Chapter 1
Vehicles Are Lazy: On Predicting Vehicle Transient Dynamics by Steady-State Responses

Sina Milani, Hormoz Marzbani, Ali Khazaei, and Reza N. Jazar

1.1 Introduction

Analysis of vehicles' handling behavior in turning maneuvers requires a proper mathematical model. There are several factors affecting a vehicle's response in a turning maneuver. Apart from variations in vehicle and tire parameters, external factors such as air resistance and slope of the road make it quite a complicated task to consider all parameters in the vehicle model. The majority of the most important features of the vehicle behavior in maneuvers are observable using fairly simplified planar vehicle models. In planar modeling, we ignore the roll, pitch, and vertical motions of the vehicle and only emphasize on the longitudinal, lateral, and yaw motions.

The most famous and basic planar vehicle model is known as the *bicycle model*. Many of the vehicle handling analyses and all the basic characterizations have been derived using bicycle model throughout the course of vehicle dynamics studies [1–3]. Bicycle model is accurate enough to represent the real car behavior to a reasonable extent in normal driving conditions. This characteristic of the bicycle model makes it useful in designing and investigating new ideas on dynamics and

S. Milani · H. Marzbani
Mechanical and Automotive Engineering, School of Engineering, RMIT University, Melbourne, VIC, Australia

A. Khazaei
Mechanical Engineering, Kennesaw State University, Marietta, GA, USA

R. N. Jazar (✉)
Xiamen University of Technology, Xiamen, China

School of Engineering, RMIT University, Bundoora, VIC, Australia
e-mail: reza.jazar@rmit.edu.au

R. N. Jazar, L. Dai (eds.), *Nonlinear Approaches in Engineering Applications*,
https://doi.org/10.1007/978-3-030-18963-1_1

control of vehicles, such as defining the nominal vehicle response for yaw-rate and/or side-slip angle [4, 5]. In the following section, the bicycle model is presented in detail and the underlying assumptions are discussed.

In the rest of the chapter, the importance of steady-state responses of the bicycle model is discussed by comparing the steady-state and transient vehicle behaviors, characteristics of maneuvering vehicles including steady-state charts are presented, and finally, application of such an analysis on a path following strategy is explained and two examples are given to evaluate the proposed idea.

1.1.1 Bicycle Model

The first step in dynamic modeling of vehicles is to identify the main forces and moments acting on the vehicle as a rigid body. The magnitude of these forces and moments depends on the motion of the vehicle, which is described by kinematic variables of the vehicle, such as longitudinal and lateral velocities, yaw rate, side-slip angles, etc. In the next step, the forces and moments must be transferred to the center of gravity of the vehicle and, finally, put into the Newton–Euler equations of motion for a rigid body on a planar surface.

The main forces acting on the vehicle are the longitudinal and lateral tire forces. There are many other acting forces and moments such as the aerodynamic forces and rolling resistance of tires which are assumed to be negligible when dealing with motion of vehicles in normal driving conditions. The normal driving condition is defined as regular turning maneuvers with forward and lateral accelerations are kept in certain limits that represent non-emergency maneuvering (see the maneuver design in Sect. 1.3).

Longitudinal tire force is a function of a kinematic variable called the longitudinal slip. The longitudinal slip is defined as the ratio of the slip velocity at tire contact patch to the longitudinal velocity of the vehicle and, therefore, is a function of tire's rotational velocity. To be able to model the longitudinal tire force, rotational dynamics of tires must be considered separately. Also, the longitudinal forces will affect the forward velocity of the vehicle, which is normally studied in vehicle performance investigations. Therefore, the longitudinal Degree of Freedom (DoF) is of less importance when dealing with turning maneuvers and is usually ignored in vehicle handling studies to avoid over-complication. Hence, the most significant external forces to be studied are the lateral tire forces. The lateral tire force is assumed to be proportional to another kinematic variable called tire side-slip angle, in normal driving condition. The tire side-slip angle α_i is defined as the angle measured from the tire's longitudinal axis x_{ti} towards the velocity vector v_i (direction of motion) at the wheel center about the vertical tire axis z_{ti} which makes a right-handed coordinate frame with x_{ti} and y_{ti} (see Fig. 1.1a) [3].

Similarly, another side-slip angle β_i may be defined for the vehicle body at any point. The body side-slip angle is defined as the angle between longitudinal axis of the vehicle body x and the velocity vector at that point v_i about the vertical body

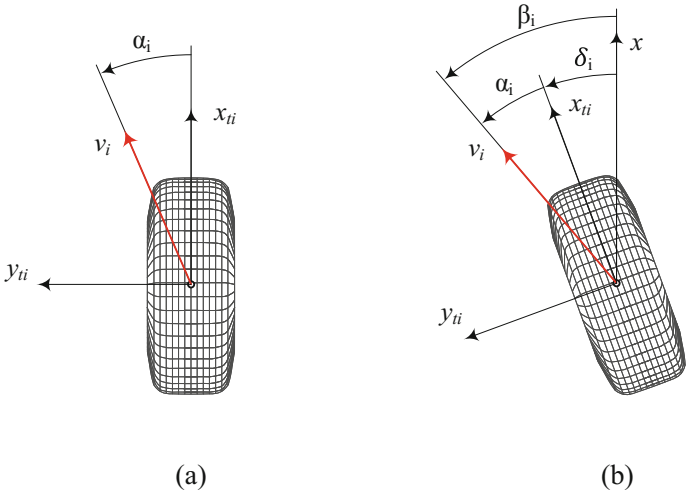

Fig. 1.1 Definition of side-slip angles and tire coordinate frame

axis z. Body side-slip angle β_i is related to longitudinal and lateral velocities of the body point expressed in vehicle body coordinate frame by (1.1). Definition of β_i allows for calculation of the tire side-slip angle for a steered wheel (see Fig. 1.1b). The tire side-slip in case of a steered wheel is obtained by the more general Eq. (1.2). One may consider steer angle of $\delta_i = 0$ for a wheel with no steering.

$$\beta_i = \arctan\left(\frac{v_{yi}}{v_x}\right) \approx \frac{v_{yi}}{v_x}, \qquad \text{for small } \beta_i \tag{1.1}$$

$$\alpha_i = \beta_i - \delta_i \approx \frac{v_{yi}}{v_x} - \delta_i \tag{1.2}$$

Note that the longitudinal velocity of any point on the vehicle body is assumed to be the same and equal to v_x in a bicycle model.

Thus, the tire lateral force is written as (1.3). The negative sign is used to match the direction of the force and the side-slip angle. When a vehicle is turning left, the lateral force is positive while the tire side-slip α_i is negative (see Fig. 1.2).

$$F_{yi} = -C_{\alpha i}\alpha_i \tag{1.3}$$

As shown in Fig. 1.2, with bicycle model of the vehicle, we assume the effect of left and right tires is lumped at the center of the axle by an equivalent tire. It is assumed that the lateral shift of the tires' vertical loads in turning maneuver is negligible and the lateral forces from left and right tires can be added up at the center of the axle. The nominal parameters of the bicycle vehicle model used in all sections of this manuscript are as follows:

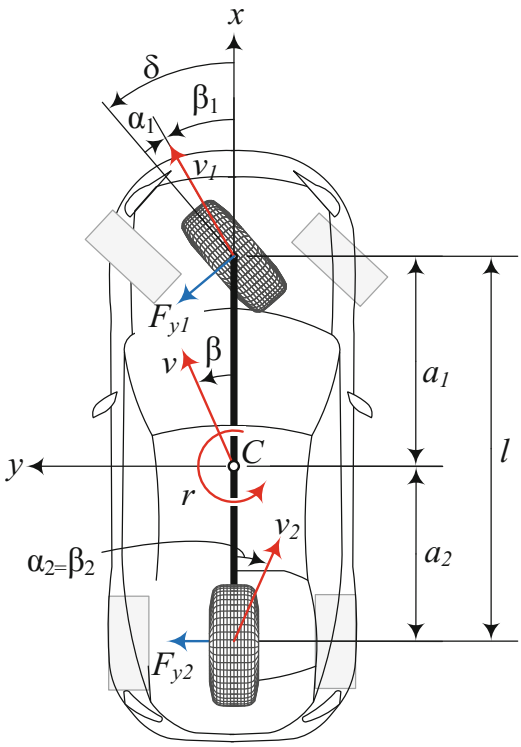

Fig. 1.2 Bicycle model and vehicle body coordinate frame

$$m = 1000\,\text{kg}$$

$$a_1 = 1\,\text{m}$$

$$a_2 = 1.5\,\text{m}$$

$$l = a_1 + a_2 = 2.5\,\text{m}$$

$$I_z = 1650\,\text{kg}\,\text{m}^2$$

$$C_{\alpha 1} = C_{\alpha 2} = 60{,}000\,\text{N/rad}$$

1.1.2 Equations of Motion

Having identified and calculated the external forces as functions of vehicle kinematic variables, we may transfer the forces to the center of gravity (point C in Fig. 1.2). Using the side-slip definition from (1.2) and assuming small δ, we may

write the total lateral force and yaw moment at vehicle's center of gravity C as (1.4), (1.5) for a front steering vehicle.

$$F_y = F_{y1} + F_{y2} = -C_{\alpha 1}\left(\frac{v_{y1}}{v_x} - \delta\right) - C_{\alpha 2}\frac{v_{y2}}{v_x} \tag{1.4}$$

$$M_z = a_1 F_{y1} - a_2 F_{y2} = -a_1 C_{\alpha 1}\left(\frac{v_{y1}}{v_x} - \delta\right) + a_2 C_{\alpha 2}\frac{v_{y2}}{v_x} \tag{1.5}$$

From the kinematics of a rigid planar vehicle, we know:

$$v_{y1} = v_y + r a_1, \qquad v_{y2} = v_y - r a_2 \tag{1.6}$$

where yaw rate r is the rotational velocity of the vehicle about z axis and v_y is the lateral velocity of the vehicle at center of gravity C along y direction. Substituting (1.6) in (1.4), (1.5), total lateral force and yaw moment become:

$$\begin{aligned} F_y &= \left(-\frac{a_1}{v_x}C_{\alpha 1} + \frac{a_2}{v_x}C_{\alpha 2}\right) r - (C_{\alpha 1} + C_{\alpha 2})\frac{v_y}{v_x} + C_{\alpha 1}\delta \\ &= C_r r + C_\beta \beta + C_\delta \delta \end{aligned} \tag{1.7}$$

$$\begin{aligned} M_z &= \left(-\frac{a_1^2}{v_x}C_{\alpha 1} - \frac{a_2^2}{v_x}C_{\alpha 2}\right) r - (a_1 C_{\alpha 1} - a_2 C_{\alpha 2})\frac{v_y}{v_x} + a_1 C_{\alpha 1}\delta \\ &= D_r r + D_\beta \beta + D_\delta \delta \end{aligned} \tag{1.8}$$

in which the *force system coefficients* $C_r, C_\beta, C_\delta, D_r, D_\beta, D_\delta$ are introduced for simplicity in the equations. These coefficients are functions of vehicle parameters, including v_x which is treated as a varying parameter.

To complete the equations of motion, we need to calculate the accelerations of the vehicle in body coordinate frame as functions of vehicle variables v_y and r. These accelerations are derived from the general Newton–Euler set of equations for 6 DoF in space. Since we limited the motion to planar, the equations simplify to longitudinal, lateral, and yaw motions [3]:

$$F_x = m(\dot{v}_x - r v_y) \tag{1.9}$$

$$F_y = m(\dot{v}_y + r v_x) \tag{1.10}$$

$$M_z = \dot{r} I_z \tag{1.11}$$

Note that the term $(\dot{v}_y + r v_x)$ is equivalent to the lateral acceleration a_y of the vehicle mass center expressed in the body frame. Equating (1.7), (1.8) with (1.10), (1.11) provides us with the equations of motion for bicycle model:

$$m(\dot{v}_y + r v_x) = C_r r + C_\beta \beta + C_\delta \delta \tag{1.12}$$

$$\dot{r} I_z = D_r r + D_\beta \beta + D_\delta \delta \tag{1.13}$$

Taking the system variables as v_y and r, we may rewrite (1.12), (1.13) in the form of a state-space representation of the system as:

$$\begin{bmatrix} \dot{v}_y \\ \dot{r} \end{bmatrix} = \begin{bmatrix} \frac{C_\beta}{m v_x} & \frac{C_r}{m} - v_x \\ \frac{D_\beta}{I_z v_x} & \frac{D_r}{I_z} \end{bmatrix} \begin{bmatrix} v_y \\ r \end{bmatrix} + \begin{bmatrix} \frac{C_\delta}{m} \\ \frac{D_\delta}{I_z} \end{bmatrix} \delta \tag{1.14}$$

Note that since we assumed v_x to be known, Eq. (1.9) does not add any information to the system dynamics; however, the required F_x obtained from the same equation provides the necessary longitudinal force during the maneuver which is assumed to be supplied.

1.1.3 Steady-State Responses

Equations of motion (1.14) may be solved numerically or analytically to obtain the transient response of bicycle model to a certain steer input δ. The same equations may also be used to derive the steady-state values of the vehicle variables v_y and r to a step steer input. In steady-state condition, all of the state variables are kept constant in time, hence, their time derivatives will be equal to zero. In other words, Eq. (1.14) reduces to (1.15) in steady-state which is solved as (1.16).

$$\begin{bmatrix} 0 \\ 0 \end{bmatrix} = \begin{bmatrix} \frac{C_\beta}{m v_x} & \frac{C_r}{m} - v_x \\ \frac{D_\beta}{I_z v_x} & \frac{D_r}{I_z} \end{bmatrix} \begin{bmatrix} (v_y)_{ss} \\ (r)_{ss} \end{bmatrix} + \begin{bmatrix} \frac{C_\delta}{m} \\ \frac{D_\delta}{I_z} \end{bmatrix} \delta \tag{1.15}$$

$$\begin{bmatrix} (v_y)_{ss} \\ (r)_{ss} \end{bmatrix} = \begin{bmatrix} \frac{C_\beta}{m v_x} & \frac{C_r}{m} - v_x \\ \frac{D_\beta}{I_z v_x} & \frac{D_r}{I_z} \end{bmatrix}^{-1} \begin{bmatrix} -\frac{C_\delta}{m} \\ -\frac{D_\delta}{I_z} \end{bmatrix} \delta \tag{1.16}$$

where "ss" subscript refers to the steady-state solution of the variables. After simplification, one may obtain v_y and r solutions as:

$$(v_y)_{ss} = \frac{D_\delta (C_r - m v_x) - D_r C_\delta}{D_r C_\beta - C_r D_\beta + m v_x D_\beta} v_x \delta \tag{1.17}$$

$$(r)_{ss} = \frac{C_\delta D_\beta - C_\beta D_\delta}{D_r C_\beta - C_r D_\beta + m v_x D_\beta}\delta \tag{1.18}$$

It can be seen that the steady-state solutions are proportional to the steer angle input. Hence, we may define steady-state responses of important vehicle variables as their ratio to the steer angle δ. To observe more details about the behavior of the vehicle in maneuver, we may introduce new dependent variables, namely body side-slip at center of gravity β, and lateral acceleration a_y which are useful in studying handling of vehicle and are defined as:

$$(\beta)_{ss} = \frac{(v_y)_{ss}}{v_x} \tag{1.19}$$

$$(a_y)_{ss} = (\dot{v}_y)_{ss} + (r)_{ss} v_x = (r)_{ss} v_x \tag{1.20}$$

Thus, the steady-state responses are obtained as:

$$S_y = \frac{(v_y)_{ss}}{\delta} = \frac{D_\delta (C_r - m v_x) - D_r C_\delta}{D_r C_\beta - C_r D_\beta + m v_x D_\beta} v_x \tag{1.21}$$

$$S_r = \frac{(r)_{ss}}{\delta} = \frac{C_\delta D_\beta - C_\beta D_\delta}{D_r C_\beta - C_r D_\beta + m v_x D_\beta} \tag{1.22}$$

$$S_\beta = \frac{(\beta)_{ss}}{\delta} = \frac{S_y}{v_x} = \frac{D_\delta (C_r - m v_x) - D_r C_\delta}{D_r C_\beta - C_r D_\beta + m v_x D_\beta} \tag{1.23}$$

$$S_a = \frac{(a_y)_{ss}}{\delta} = S_r v_x = \frac{C_\delta D_\beta - C_\beta D_\delta}{D_r C_\beta - C_r D_\beta + m v_x D_\beta} v_x \tag{1.24}$$

Note that the lateral and centripetal accelerations are approximately equal for small side-slip angle β and forward acceleration a_x, but in general, the following relationship is held between a_c, a_x, a_y:

$$\begin{aligned} a_c &= a_y \cos\beta - a_x \sin\beta \\ &\approx a_y \qquad \text{if } (a_x \,\&\, \beta \text{ small}) \end{aligned} \tag{1.25}$$

$$a_x = \dot{v}_x - r v_y \tag{1.26}$$

$$a_y = \dot{v}_y + r v_x \tag{1.27}$$

Denominator of (1.21)–(1.24) forms the characteristic equation of the dynamic system. A combination of the vehicle parameters dictates the general behavior of the vehicle. Substituting the vehicle parameters into the force system coefficients, the denominator D is obtained; equating it to zero, we may find a stability condition for turning maneuver:

$$D = m(C_{\alpha 2}a_2 - C_{\alpha 1}a_1)v_x^2 + l^2 C_{\alpha 1}C_{\alpha 2} = 0 \tag{1.28}$$

$$\frac{m}{l^2}\left(\frac{a_2}{C_{\alpha 1}} - \frac{a_1}{C_{\alpha 2}}\right)v_x^2 + 1 = K v_x^2 + 1 = 0 \tag{1.29}$$

$$v_x = v_c = \sqrt{-\frac{1}{K}} \tag{1.30}$$

$$K = \frac{m}{l^2}\left(\frac{a_2}{C_{\alpha 1}} - \frac{a_1}{C_{\alpha 2}}\right) \tag{1.31}$$

where v_c is the critical speed at which the denominator will become zero and the vehicle becomes unstable. The critical speed only exists when the stability factor K is negative. The stability factor determines whether the vehicle is *under-steer* ($K > 0$), *over-steer* ($K < 0$), or *neutral-steer* ($K = 0$). The behavior of the vehicle changes with different signs of K which is not in the scope of this chapter. For more information about the effect of K on vehicle responses, see [1–3].

1.2 Center of Curvature and Path of Motion

One of the main characteristics of a maneuvering vehicle which is emphasized in this chapter is the path of motion. The path of motion is directly related to the radius of turning R and the center of curvature of the vehicle at each time instance, which is also called the Instantaneous Center of Rotation (ICR). In this section, the methodology to calculate R and ICR as well as obtaining the global vehicle coordinates (X, Y) which define the path of motion will be examined. Calculation of ICR helps in understanding the similarity between transient and steady-state responses [6]. The usage of the presented calculations is detailed in Sect. 1.3.

1.2.1 Curvature and Turning Radius

We start by calculating the radius of turning R. For a particle rotating about a center with radius R, translational velocity of v, and angular velocity of ω, in 2-dimensional space, the following relationship holds:

$$v = R\omega \tag{1.32}$$

The relation between longitudinal and lateral velocities v_x, v_y and the body side-slip angle β can be written as:

$$v = v_x \cos\beta + v_y \sin\beta \tag{1.33}$$

and since β is assumed to be small:

$$v = v_x + v_y\beta \tag{1.34}$$

Assuming the vehicle to be a point mass at its mass center rotating with angular velocity of $\omega = r$, we may use (1.32) and (1.34) to write:

$$R = \frac{v}{r} = \frac{v_x + v_y\beta}{r} \tag{1.35}$$

$$\kappa = \frac{1}{R} = \frac{r}{v_x + v_y\beta} \tag{1.36}$$

where κ is called the *curvature of the path* and R is the radius of curvature. For straight driving, $\kappa = 0$ while $R \to \infty$. Using (1.36) and substituting v_y, r, β from (1.21)–(1.23), we may obtain the value of κ in steady-state which would be a nonlinear function of steer input δ. On the other hand, the multiplication of two small quantities v_y and β is negligible compared to v_x in (1.35), (1.36). So, with a highly reasonable approximation, we may ignore the term $v_y\beta$ in (1.35), (1.36) and rewrite them as:

$$R = \frac{v}{r} = \frac{v_x}{r} \tag{1.37}$$

$$\kappa = \frac{1}{R} = \frac{r}{v_x} \tag{1.38}$$

By using (1.37), (1.38) instead of (1.35), (1.36), we end up with a linear relationship between $(\kappa)_{ss}$ and δ and we are able to define an additional steady-state response S_κ called the *curvature response*:

$$(\kappa)_{ss} = \frac{1}{(R)_{ss}} = \frac{(r)_{ss}}{v_x} \tag{1.39}$$

$$S_\kappa = \frac{(\kappa)_{ss}}{\delta} = \frac{S_r}{v_x} = \frac{C_\delta D_\beta - C_\beta D_\delta}{(D_r C_\beta - C_r D_\beta + m v_x D_\beta) v_x} \tag{1.40}$$

The importance of the curvature and its steady-state response in analyzing vehicle's maneuver is due to its key role in calculating ICR as explained in the following sections.

1.2.2 ICR in Vehicle Body Coordinate Frame

Having the radius of curvature R calculated, we know how far ICR is located from vehicle's center of gravity. On the other hand, the vehicle side-slip angle determines how much rotation exists between the vehicle's heading direction and the direction

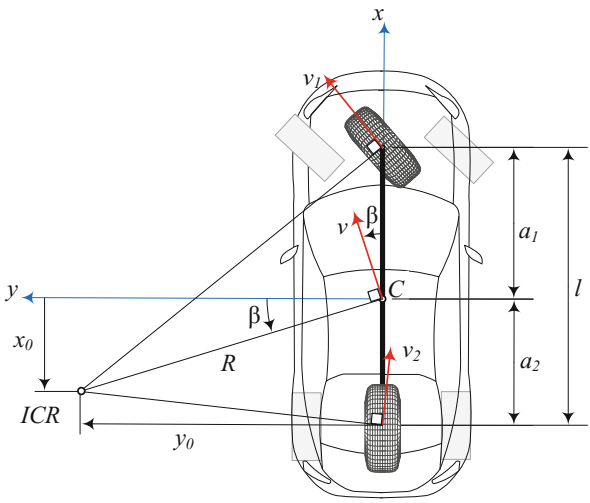

Fig. 1.3 Location of ICR in vehicle body frame

tangent to the path. Thus, the side-slip angle β affects the longitudinal and lateral coordinates of ICR (x_0, y_0) in body frame. Figure 1.3 shows the calculation of ICR location in the vehicle body coordinate frame.

Thus, x_0 and y_0 are calculated as:

$$x_0 = -R \sin \beta \tag{1.41}$$

$$y_0 = R \cos \beta \tag{1.42}$$

Note that we do not use small angle approximation here to be able to observe both the lateral and longitudinal location of ICR in the body coordinate frame.

1.2.3 ICR in Global Coordinate Frame

The location of ICR may also be calculated in the global coordinate frame. The relationship between global and body coordinate frames is defined using the rotation matrix ${}^{G}R_{B}$. Any position vector in 3-dimensional space may be expressed whether in global frame G shown by ${}^{G}\vec{d}$ or in body frame B shown by ${}^{B}\vec{d}$. Transformation between body to global coordinate is defined by [7]:

$${}^{G}\vec{d} = {}^{G}R_{B}\,{}^{B}\vec{d} + {}^{G}\vec{e}_{BG} \tag{1.43}$$

$${}^{G}R_{B} = \begin{bmatrix} \cos\psi & -\sin\psi & 0 \\ \sin\psi & \cos\psi & 0 \\ 0 & 0 & 1 \end{bmatrix} \tag{1.44}$$

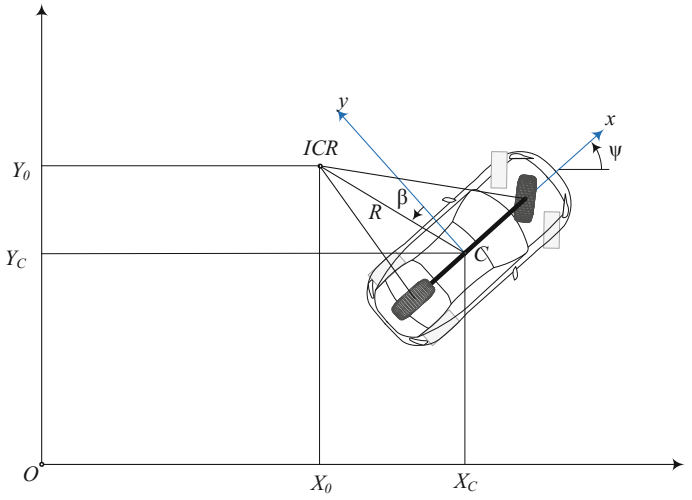

Fig. 1.4 Location of ICR in global frame

where ${}^{G}\vec{e}_{BG}$ is the position vector of the origin of body frame O_B with respect to the origin of the global frame O_G expressed in global frame G; and ψ is the heading angle of the vehicle which is measured from the global longitudinal axis X towards vehicle's longitudinal axis x about the vertical axis z. In case of a vehicle in turning maneuver, ${}^{G}\vec{e}_{BG}$ is defined by global position components of the vehicle's center of gravity X_C, Y_C. Figure 1.4 shows the global position and orientation of the vehicle in a turning maneuver.

Applying the transformation (1.43) from body frame to global frame for ICR position vector yields:

$$\begin{bmatrix} X_0 \\ Y_0 \\ 0 \end{bmatrix} = \begin{bmatrix} \cos\psi & -\sin\psi & 0 \\ \sin\psi & \cos\psi & 0 \\ 0 & 0 & 1 \end{bmatrix} \begin{bmatrix} x_0 \\ y_0 \\ 0 \end{bmatrix} + \begin{bmatrix} X_C \\ Y_C \\ 0 \end{bmatrix} \tag{1.45}$$

$$X_0 = x_0 \cos\psi - y_0 \sin\psi + X_C \tag{1.46}$$

$$Y_0 = x_0 \sin\psi + y_0 \cos\psi + Y_C \tag{1.47}$$

substituting from (1.41), (1.42) the global coordinates of ICR are obtained as:

$$X_0 = -R \sin\beta \cos\psi - R \cos\beta \sin\psi + X_C \tag{1.48}$$

$$Y_0 = -R \sin\beta \sin\psi + R \cos\beta \cos\psi + Y_C \tag{1.49}$$

Calculation of the global coordinates X_C, Y_C which construct the path of motion is presented in the following section.

1.2.4 Path of Motion

We may assume that the vehicle was initially coincident with the origin of the global frame. As the vehicle moves, a combination of the longitudinal, lateral, and yaw velocities causes displacement and change of direction with respect to the global frame. To calculate the current global coordinates at any time, we need to integrate the velocities expressed in global frame, namely $\dot{X}_C = v_X$, $\dot{Y}_C = v_Y$. On the other hand, these velocities are related to local expressions of the velocities in body frame, namely v_x, v_y through a rotation of ψ about the vertical axis z. The transformation between local and global velocity vectors is defined by:

$$^{G}v = {}^{G}R_{B}\,{}^{B}v \tag{1.50}$$

$$\begin{bmatrix} \dot{X}_C \\ \dot{Y}_C \end{bmatrix} = \begin{bmatrix} \cos\psi & -\sin\psi & 0 \\ \sin\psi & \cos\psi & 0 \\ 0 & 0 & 1 \end{bmatrix} \begin{bmatrix} v_x \\ v_y \end{bmatrix} \tag{1.51}$$

$$\dot{X}_C = v_x \cos\psi - v_y \sin\psi \tag{1.52}$$

$$\dot{Y}_C = v_x \sin\psi + v_y \cos\psi \tag{1.53}$$

As (1.52) and (1.53) imply, derivation of the path of motion relies on calculation of heading angle ψ. On the other hand, time derivative of ψ is equal to the yaw velocity of the vehicle r:

$$\dot{\psi} = r \tag{1.54}$$

Using the expressions (1.52)–(1.54), we may increase the order of the system expressed by (1.14) and introduce new state variables X_C, Y_C, ψ in order to obtain the integrated quantities required for plotting the path, as outputs of the system. This way, any numerical integration method used for solving the differential equations of the system will also result in the path of motion. Augmenting the system variables in (1.14) by (1.52)–(1.54), the new system would be represented by the following set of differential equations:

$$\begin{bmatrix} \dot{v}_y \\ \dot{r} \\ \dot{X}_C \\ \dot{Y}_C \\ \dot{\psi} \end{bmatrix} = \begin{bmatrix} \frac{C_\beta}{m v_x} & \frac{C_r}{m} - v_x & 0 & 0 & 0 \\ \frac{D_\beta}{I_z v_x} & \frac{D_r}{I_z} & 0 & 0 & 0 \\ -\sin\psi & 0 & 0 & 0 & 0 \\ \cos\psi & 0 & 0 & 0 & 0 \\ 0 & 1 & 0 & 0 & 0 \end{bmatrix} \begin{bmatrix} v_y \\ r \\ X_C \\ Y_C \\ \psi \end{bmatrix} + \begin{bmatrix} \frac{C_\delta}{m}\delta \\ \frac{D_\delta}{I_z}\delta \\ v_x \cos\psi \\ v_x \sin\psi \\ 0 \end{bmatrix} \tag{1.55}$$

Note that the above system is nonlinear due to potentially large values of ψ making it impossible to linearly approximate $\sin\psi$ and $\cos\psi$ terms.

1.3 Comparing Transient and Steady-State Behaviors

Steady-state relations may be used to calculate settled responses while the differential equations must be solved to obtain the transient responses. Road vehicles are most of the time performing in a steady-state condition. In all other times, the vehicle is undergoing a transition between two steady-states. Such a transition in normal driving conditions is examined in this section. The objective of this section is to show how this transition is made and how far the vehicle responses deviate from quasi-steady-state transition. A Quasi-Steady-State (QSS) transition happens when the inputs to the vehicle change at very low rates such that the vehicle responses are close to steady-state responses at each time instance. The laziness in vehicle's behavior is defined by "vehicle's tendency to get to the steady-state condition as soon as possible." Two different maneuver types are investigated in this manuscript to examine the vehicle's laziness against input changes during a turning maneuver: 1—increasing forward velocity at constant steering, and 2—increasing steer angle at constant forward velocity.

In designing the maneuvers, the maximum longitudinal acceleration is set to be $a_{x\cdot\max} = \pm 7.5\,\mathrm{m/s^2}$ since the maximum achievable acceleration or deceleration for a vehicle with perfect traction management is $a_x = \pm\mu g$ and for a passenger vehicle $\mu \approx 0.75$. Maximum lateral acceleration is set at $a_{y\cdot\max} = \pm 0.5\,\mathrm{g} = \pm 4.91\,\mathrm{m/s^2}$. Such a limitation avoids creation of large angles and considerable lateral load shift in order for the bicycle model to remain valid. Both longitudinal and lateral accelerations are well-above the limits of regular driving with passenger vehicles.

1.3.1 Time Response of System Variables

In this section, we examine the time responses of the main vehicle variables in time domain and see how they behave in transient and steady-state conditions. As (1.14) implies, the lateral velocity v_y and yaw velocity r are the main variables of the vehicle system. It is also useful to monitor the lateral acceleration of the vehicle a_y. Lateral acceleration is approximately equal to the centripetal acceleration of the vehicle in a turning maneuver when side-slip angle β is small, and it is an indication of lateral tire forces. To start examining the laziness of vehicles in maneuvers, we may start by calculating the QSS response of the above-mentioned variables between two steady-state conditions.

Using the vehicle parameters provided in Sect. 1.1.1, we first calculate the force system coefficients in (1.7), (1.8), and then all of the steady-state responses in (1.21)–(1.24) and (1.40) are evaluated for the corresponding range of v_x and δ:

$$C_r = -\frac{30{,}000}{v_x}\,\mathrm{N/rad} \tag{1.56}$$

$$C_\beta = -120{,}000\,\mathrm{N/rad} \tag{1.57}$$

$$C_\delta = 60{,}000\,\mathrm{N/rad} \tag{1.58}$$

$$D_r = -\frac{195{,}000}{v_x}\,\mathrm{Nm/rad} \tag{1.59}$$

$$D_\beta = 30{,}000\,\mathrm{Nm/rad} \tag{1.60}$$

$$D_\delta = 60{,}000\,\mathrm{Nm/rad} \tag{1.61}$$

$$S_y = -\frac{2v_x(v_x^2 - 225)}{v_x^2 + 750}\,\mathrm{m/s\,rad} \tag{1.62}$$

$$S_r = \frac{300v_x}{v_x^2 + 750}\,\mathrm{rad/s\,rad} \tag{1.63}$$

$$S_\beta = -\frac{2v_x^2 - 450}{v_x^2 + 750}\,\mathrm{rad/rad} \tag{1.64}$$

$$S_a = \frac{300v_x^2}{v_x^2 + 750}\,\mathrm{m/rad\,s^2} \tag{1.65}$$

$$S_\kappa = \frac{300}{v_x^2 + 750}\,\mathrm{1/m\,rad} \tag{1.66}$$

For transient simulation, system (1.14), or alternatively (1.55), is solved numerically for v_y and r. The lateral acceleration in transient maneuver can be calculated from (1.10) as:

$$a_y = \dot{v}_y + r v_x \tag{1.67}$$

where $\dot{v}_y$ is found from (1.14) as:

$$\dot{v}_y = \frac{C_\beta}{m v_x} v_y + \left(\frac{C_r}{m} - v_x\right) r + \frac{C_\delta}{m}\delta \tag{1.68}$$

substituting in (1.67):

$$a_y = \frac{1}{m}\left(\frac{C_\beta}{v_x} v_y + C_r r + C_\delta \delta\right) \tag{1.69}$$

Equivalently, we may obtain a_y directly from (1.7) as:

$$a_y = \frac{1}{m} F_y = \frac{1}{m} \left(C_\beta \beta + C_r r + C_\delta \delta \right) \tag{1.70}$$

Manuver 1: Increasing Velocity

The first maneuver consists of both increasing and decreasing the forward velocity v_x at the rate of maximum longitudinal acceleration, while keeping the steer angle δ constant. The maneuver starts from an initial velocity of $v_{x0} = 10\,\text{m/s}$ with a large constant large acceleration of $a_{x\cdot\max} = 7.5\,\text{m/s}^2$ up to $v_{x1} = 25\,\text{m/s}$ in 2 s. After another 2 s (to ensure reaching steady-state) vehicle then decelerates at the opposite rate back to $v_{x2} = 10\,\text{m/s}$ in 2 s. The maneuver continues up to $t = 8\,\text{s}$ to ensure reaching steady-state. We may then calculate the constant steer angle at which the maximum lateral acceleration of $a_{y\cdot\max} = 4.91\,\text{m/s}^2$ is created in the middle of the maneuver:

$$\delta = \frac{a_{y\cdot\max}}{S_{a1}} = \frac{4.91}{136.36} = 0.036\,\text{rad} = 2.06\,\text{deg} \tag{1.71}$$

Inputs are plotted in Fig. 1.5.

The initial values of the variables v_y, r are set to their steady-state values at v_{x0} to realize the first steady-state condition at the beginning of the maneuver when solving the differential equations of motion:

$$v_{y0} = S_{y0}\delta = (2.94)(0.036) = 0.11\,\text{m/s} \tag{1.72}$$

$$r_0 = S_{r0}\delta = (3.53)(0.036) = 0.13\,\text{rad/s} \tag{1.73}$$

Figure 1.6 shows the variation of lateral velocity v_y in the QSS case (gradual increase of v_x) as well as the transient response. The difference between the two is

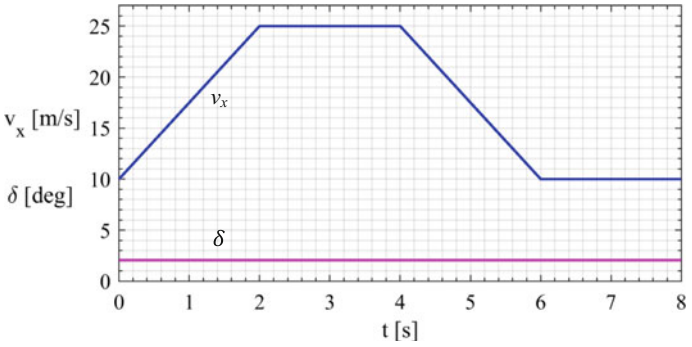

Fig. 1.5 Steering and velocity inputs for maneuver 1

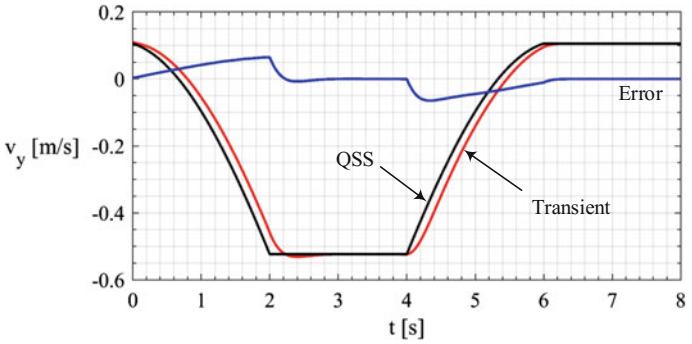

Fig. 1.6 QSS versus transient response of v_y for increasing v_x at constant δ

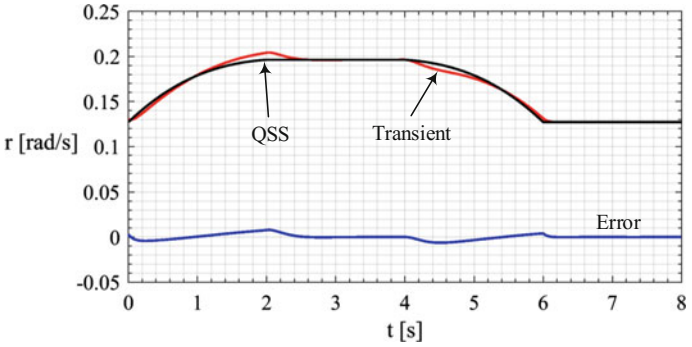

Fig. 1.7 QSS versus transient response of r for increasing v_x at constant δ

also plotted as the error. The plot shows a reasonable level of error at each time. Error magnitude is larger at higher velocities, but settles very quickly when motion becomes steady. It is also observed that the transient curve of v_y is slightly shifted (about 0.2 s) in time domain which is negligible compared to the response time, indicating the laziness of v_y response in this maneuver, both for acceleration and deceleration.

Figure 1.7 depicts the variation of yaw velocity r for both conditions. Maximum error between transient and QSS responses is observed at around $t = 2$ right at the end of transition to higher velocity, but it shows very quick elimination of the error and drop of the yaw velocity to its steady-state in around 0.5 s afterwards. Yaw velocity shows a very similar response to the QSS.

The lateral acceleration plot is shown in Fig. 1.8. It can be seen that the deviation between the responses is almost uniform during transition and it does not exceed $0.2\,\mathrm{m/s^2}$ which is around 4% of the maximum acceleration during such a quick transition, proving a close response to QSS.

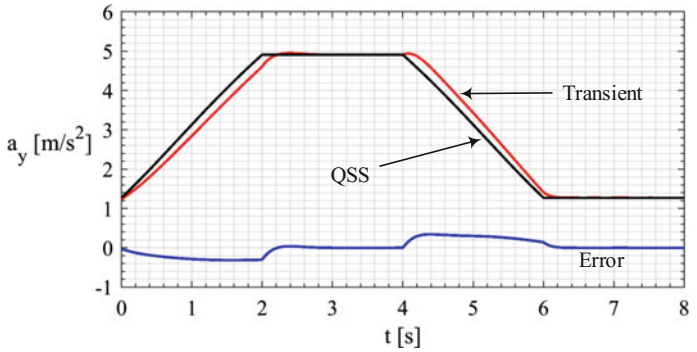

Fig. 1.8 QSS versus transient response of a_y for increasing v_x at constant δ

Maneuver 2: Increasing Steer Angle

The second maneuver is defined as increasing steer angle δ at constant velocity of $v_x = 20\,\text{m/s}$ from an initial value of $\delta_0 = 0$ with constant rate of $1\,\text{deg/s}$ up to the final value of δ_1. The final value of the steer angle is calculated such that the final lateral acceleration is approximately equal to $a_y \approx a_{y\cdot\max} = 4.91\,\text{m/s}^2$ as the limiting value.

$$\delta_1 = \frac{a_{y\cdot\max}}{S_{a1}} = \frac{4.91}{104.35} = 0.047\,\text{rad} = 2.70\,\text{deg} \tag{1.74}$$

$$t_1 = \frac{\delta_1 - \delta_0}{1} = 2.7\,\text{s} \tag{1.75}$$

Similar to the previous maneuver, the initial values of the variables v_y, r are set to their steady-state values at δ_1 to realize the first steady-state condition at the beginning of the maneuver:

$$v_{y0} = S_{y0}\delta_0 = 0\,\text{m/s} \tag{1.76}$$

$$r_0 = S_{r0}\delta_0 = 0\,\text{rad/s} \tag{1.77}$$

The simulation continues up to $t = 5\,\text{s}$ after $t = t_1$ to damp any transient behavior. Velocity and steer inputs are plotted in Fig. 1.9.

Variation of v_y for QSS and transient maneuvers for the second maneuver are shown in Fig. 1.10. It is observed that the transient value of v_y shows less agreement with QSS response, indicating some expected side-slip difference between transient and QSS during the transition. However, the effect of v_y in total velocity v is negligible.

Variation of yaw velocity r is shown in Fig. 1.11. There is a high level of agreement between plots and the steady-state behavior seems to be dominant.

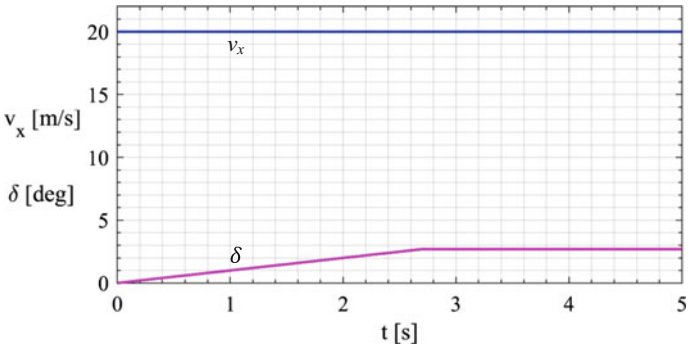

Fig. 1.9 Steering and velocity inputs for maneuver 2

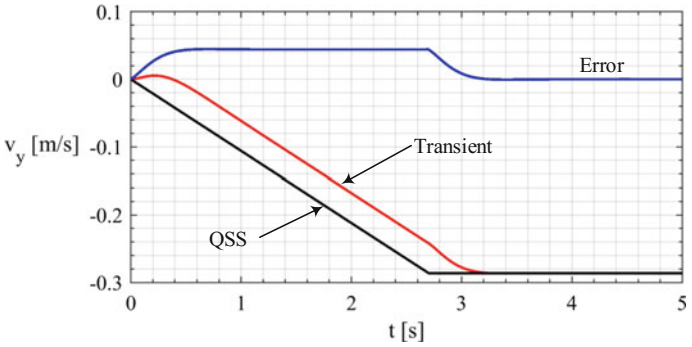

Fig. 1.10 QSS versus transient response of v_y for increasing δ at constant v_x

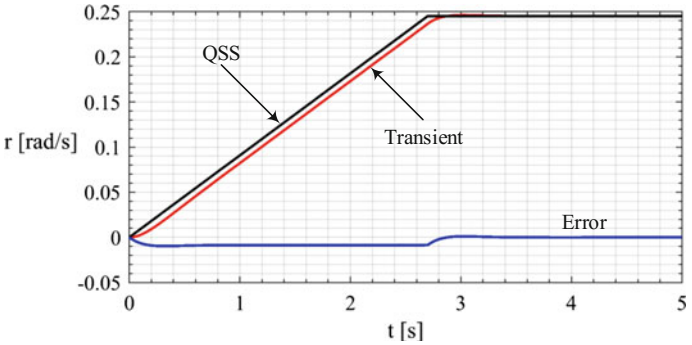

Fig. 1.11 QSS versus transient response of r for increasing δ at constant v_x

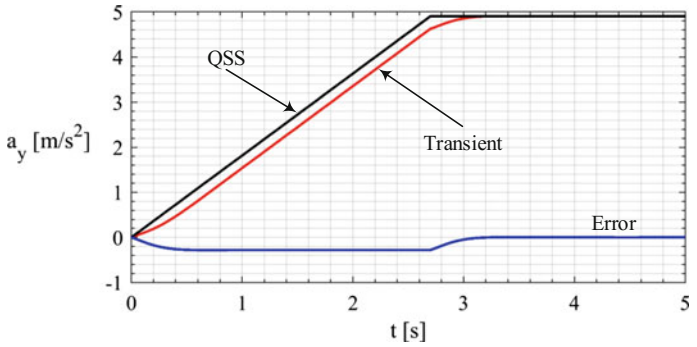

Fig. 1.12 QSS versus transient response of a_y for increasing δ at constant v_x

Figure 1.12 shows how the lateral acceleration varies during the maneuver in transient and QSS conditions. Similar to yaw velocity, the lateral acceleration response shows a high tendency to QSS case, proving laziness of the vehicle with respect to a_y.

Steady-State Surface Maps

It was shown in sections "Manuver 1: Increasing Velocity" and "Maneuver 2: Increasing Steer Angle" that the time response of the vehicle variables is close to their QSS responses. Although v_x is a varying parameter of system (1.14), we may also treat the steer angle δ and the forward velocity v_x as the inputs from the driver to the vehicle system. Having v_x and δ as inputs and using the conclusion above, we may introduce 3-dimensional surfaces consisting of steady-state variables $(v_y)_{ss}, (r)_{ss}, (a_y)_{ss}$ for each pair of v_x, δ. Such a surface is called a *steady-state surface map* of the variable of interest which indicates the steady-state value of that variable in the input domain, instead of time domain.

We expect the transient response plots to lie very close to the steady-state surface maps, because of the transient time response of the vehicle being close to its QSS response. To plot the surface maps, we create a mesh for a range of v_x and a range of δ values and calculate the steady-state variable for each point.

Figures 1.13, 1.14, and 1.15 show the steady-state surface maps for v_y, r, a_y respectively. They include full information about all possible responses of variables with any set of inputs. It is important to note that surface maps do not include any information about the time. To find the time duration in which the transient results are obtained, one must refer to the definition of the input as a function of time, presented in sections "Manuver 1: Increasing Velocity" and "Maneuver 2: Increasing Steer Angle".

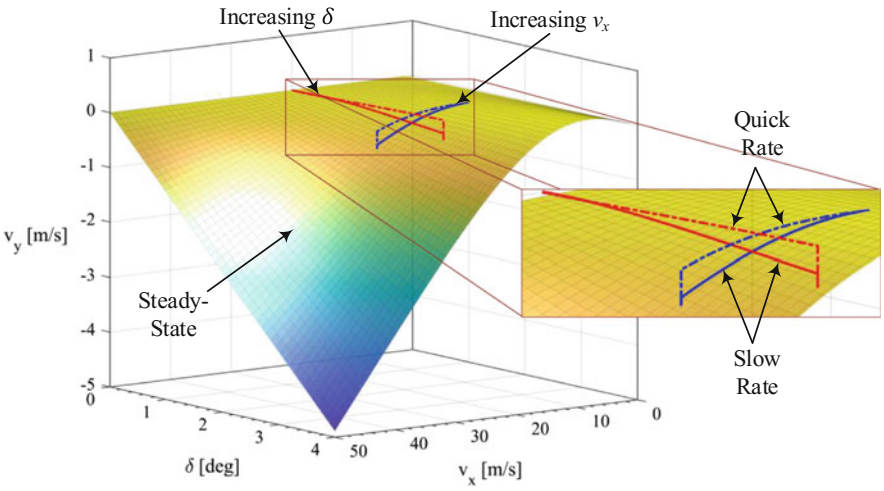

Fig. 1.13 Steady-state surface map of v_y

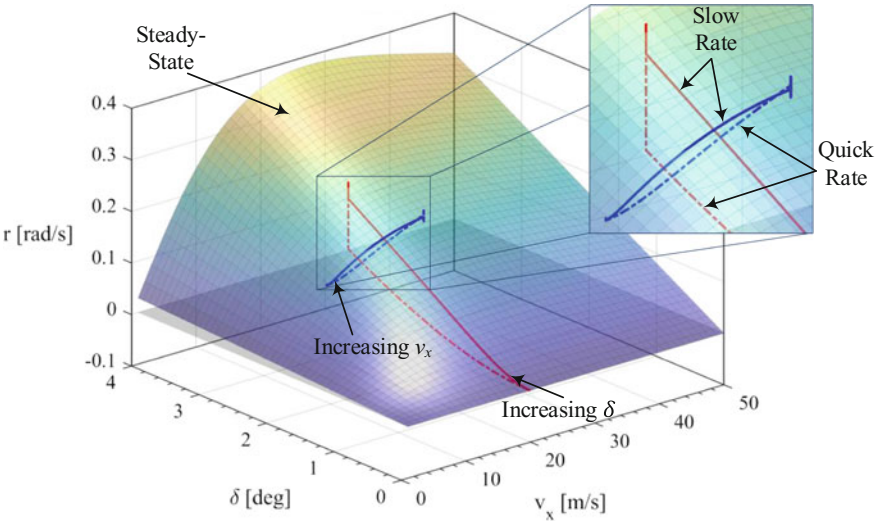

Fig. 1.14 Steady-state surface map of r

Similar to sections "Manuver 1: Increasing Velocity" and "Maneuver 2: Increasing Steer Angle", two maneuvers of increasing $v_x : 10 \rightarrow 25\,\text{m/s}$ at $\delta = 2.06\,\text{deg}$ in two different time durations of 2 s and 4 s are plotted by the blue curves. Another maneuver of increasing $\delta : 0 \rightarrow 2.7\,\text{deg}$ at $v_x = 20\,\text{m/s}$ in two different time durations of 1 s and 2 s is plotted by the red curves. As expected, it is observed that as the time duration of the transition between two steady-state cases gets smaller, the transient behavior becomes more visible and the deviation of the transient plot

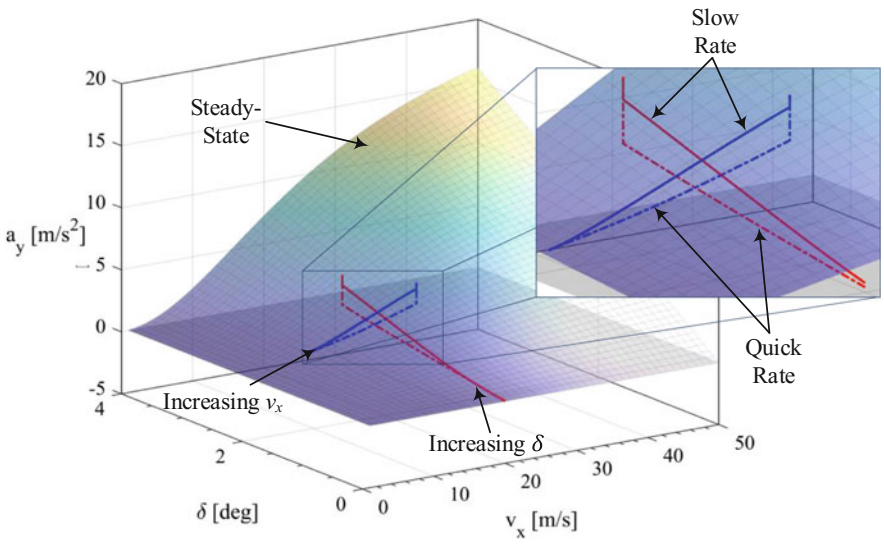

Fig. 1.15 Steady-state surface map of a_y

from steady-state surface map increases. Nevertheless, it can be seen that even the limiting quick maneuver lies reasonably close to the steady-state surface.

Although the focus of this manuscript is on investigating maneuvers with only v_x or δ being variable to assess the sensitivity with respect to each input, let us consider a special case of decreasing steer angle δ and increasing velocity v_x at the same time, which represents a condition of merging into a new road. The transient response of such a maneuver with $\delta : 3\,\text{deg} \rightarrow 0\,\text{deg}$ and $v_x : 10\,\text{m/s} \rightarrow 30\,\text{m/s}$ in 3 s is plotted in Fig. 1.16. It can be seen that the response of this maneuver is also very close to the steady-state.

1.3.2 Center of Curvature Response (ICR Map)

So far, the responses of vehicle body variables are investigated and found to be acting close to their steady-state values in normal driving conditions. It is expected that such a lazy behavior will also be observable in the location of ICR. If we are able to reasonably approximate the location of ICR by steady-state calculation, we may directly relate the ICR response of a certain vehicle only to steer input and forward velocity of that vehicle at any time instance. Hence, we can generate a look-up table for vehicle turning maneuver so that any feasible turning demand (ICR location in body coordinate frame) is translated to a pair of (v_x, δ) for autonomous maneuvering of vehicles.

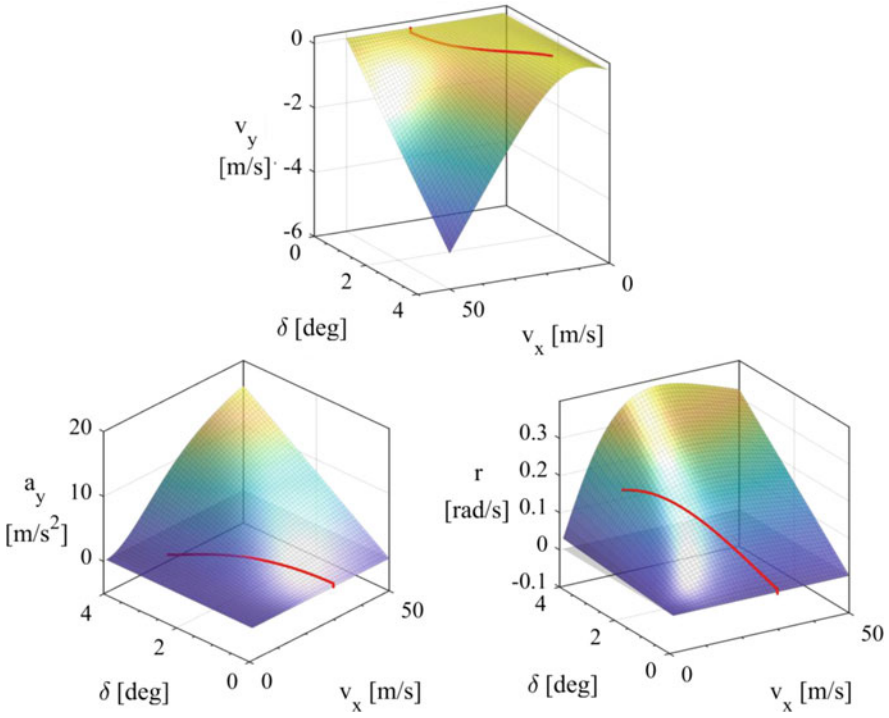

Fig. 1.16 Steady-state surface maps for special maneuver of turning into a road

For a pair of (v_x, δ), the steady-state ICR coordinates in body frame are calculated using (1.41), (1.42):

$$(x_0)_{ss} = -(R)_{ss} \sin(\beta)_{ss} = -\frac{1}{\delta S_\kappa} \sin(\delta S_\beta) \tag{1.78}$$

$$(y_0)_{ss} = (R)_{ss} \cos(\beta)_{ss} = \frac{1}{\delta S_\kappa} \cos(\delta S_\beta) \tag{1.79}$$

Considering specific ranges for v_x and r, a steady-state chart is calculated that contains all the possible ICR locations in body coordinate. Such a chart is called the *ICR map*. Figure 1.17 shows the ICR map for the vehicle of interest in this manuscript for prescribed ranges of v_x, δ.

In Fig. 1.17, the horizontal black lines indicate constant velocity curves and the green lines indicate constant steer angle curves. Note that these curves are nonlinear functions of v_x and δ as expressions (1.78), (1.79) imply, but the range of feasible input values v_x, δ, limits the curves to regions in which they look linear. For any point in between the plotted points, an interpolation may be used to calculate the required (v_x, δ). Analytical calculations are also possible for higher accuracy.

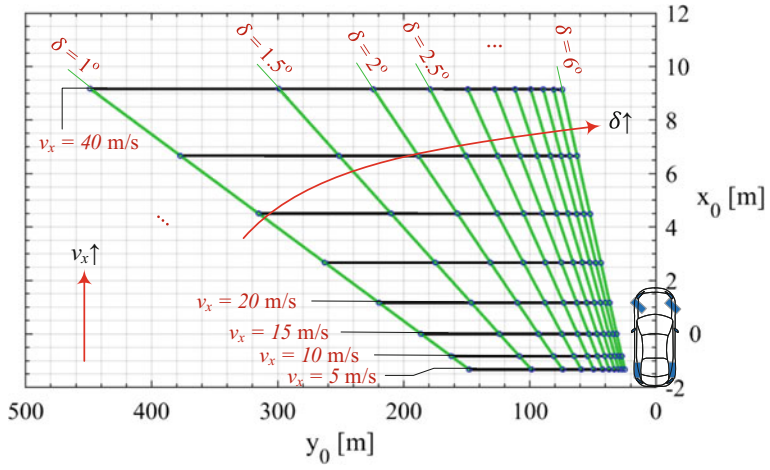

Fig. 1.17 ICR map (loci of possible steady-state ICRs in body coordinate)

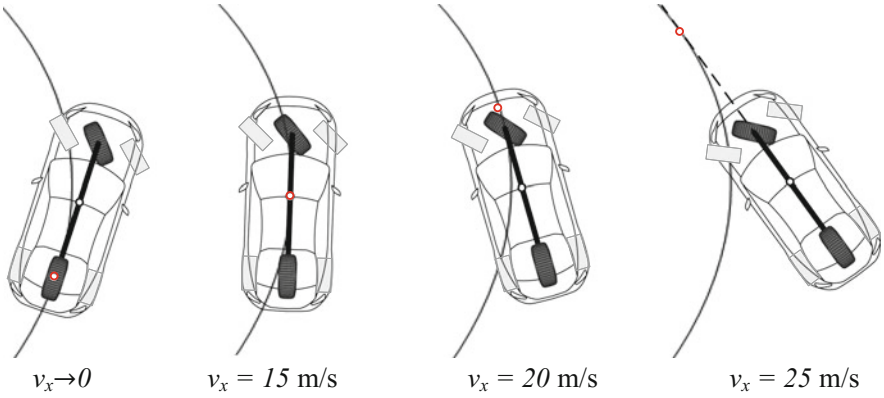

Fig. 1.18 Variation of the tangent point at different velocities

Figure 1.17 indicates that at a certain forward velocity, the longitudinal position of ICR is almost constant for any steer angle. Connecting the point ${}^{B}(x_0, 0)$ in the body coordinate to ICR, we can conclude that the velocity of the body at that point is perpendicular to the radius of curvature and tangent to x. In other words, the point ${}^{B}(x_0, 0)$ is the only point on the body frame that travels tangent to the path. Such a location is called the *tangent point*. Figure 1.18 shows how the tangent point varies at different velocities.

At very low velocities (kinematic turning), the tangent point is on the extension of the rear axle. As the speed increases, the tangent point reaches the center of gravity ($\beta = 0$); this velocity at which the side-slip angle becomes zero is also called the

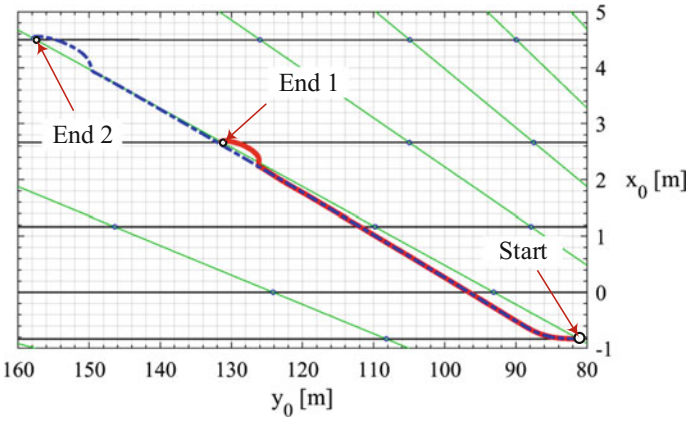

Fig. 1.19 Variation of ICR in body coordinate: effect of Δv_x magnitude at constant δ

tangent speed [2]. It moves further forward with increasing speed. Note that the tangent point is not necessarily on the vehicle body and it may go further beyond the size of actual vehicle body. The tangent point does not go behind the rear axle when the vehicle is moving forward.

Let us compare characteristic transient maneuvers with ICR map to see how the magnitude and the rate of change in the inputs affect the location of ICR when compared to steady-state.

Figure 1.19 shows two different scenarios applied on the same vehicle at constant steer angle of $\delta = 2\,\text{deg}$. The first scenario represents an increase of velocity from $v_{x0} = 10\,\text{m/s}$ to $v_{x1} = 25\,\text{m/s}$ in 2 s. The second scenario represents an increase of velocity from $v_{x0} = 10\,\text{m/s}$ to $v_{x1} = 30\,\text{m/s}$ in 2.7 s. Note that the rate of change in forward velocity is equal for both scenarios. It is observed that, as the rate is equal in both cases, the proximity to QSS is almost equal, but the larger magnitude of Δv_x in the second scenario causes more time of deviation between transient and QSS. Hence, the smaller the change in Δv_x, the lazier the vehicle would be.

Figure 1.20 shows two different scenarios applied on the same vehicle at constant steer angle of $\delta = 2\,\text{deg}$. The first scenario represents an increase of velocity from $v_{x0} = 10\,\text{m/s}$ to $v_{x1} = 25\,\text{m/s}$ in 2 s. The second scenario represents the same increase of velocity in 1 s. It is observed that, as the magnitude of change is equal in both cases, the beginning and end points are the same in both scenarios, but the larger rate of $\Delta v_x/\Delta t$ in the second scenario causes more deviation of transient from QSS. Hence, the smaller the rate of change $\Delta v_x/\Delta t$, the lazier the vehicle would be.

Figure 1.21 shows two different scenarios applied on the same vehicle at constant velocity of $v_x = 20\,\text{m/s}$. The first scenario represents an increase of steer angle from $\delta_0 = 1\,\text{deg}$ to $\delta_1 = 2\,\text{deg}$ in 1 s. The second scenario represents an increase of steer angle from $\delta_0 = 1\,\text{deg}$ to $\delta_1 = 3\,\text{deg}$ in 2 s. Note that the rate of change in steer angle is equal for both scenarios. It is observed that, as the rate is equal in both

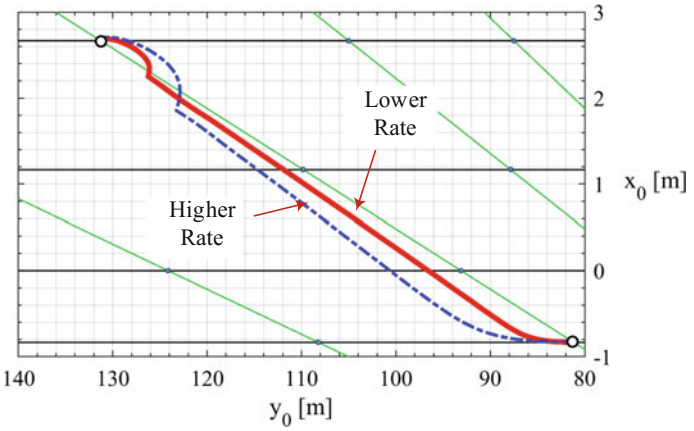

Fig. 1.20 Variation of ICR in body coordinate: effect of $\Delta v_x/\Delta t$ rate at constant δ

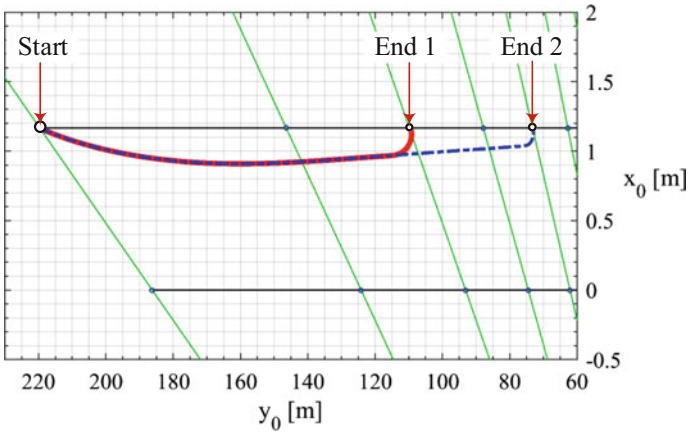

Fig. 1.21 Variation of ICR in body coordinate: effect of $\Delta\delta$ magnitude at constant v_x

cases, the proximity to QSS is almost equal, but the larger magnitude of $\Delta\delta$ in the second scenario causes more time of deviation between transient and QSS. Hence, the smaller the change in $\Delta\delta$, the lazier the vehicle would be.

Figure 1.22 shows two different scenarios applied on the same vehicle at constant velocity of $v_x = 20\,\text{m/s}$. The first scenario represents an increase of steer angle from $\delta_0 = 1\,\text{deg}$ to $\delta_1 = 2\,\text{deg}$ in 1 s. The second scenario represents the same increase of steer angle in 0.5 s. Magnitude of change is equal in these cases, the beginning and end points are the same in both scenarios, but the larger rate of $\Delta\delta/\Delta t$ in the second scenario causes more deviation of transient from QSS. Hence, the smaller the rate of change $\Delta\delta/\Delta t$, the lazier the vehicle would be.

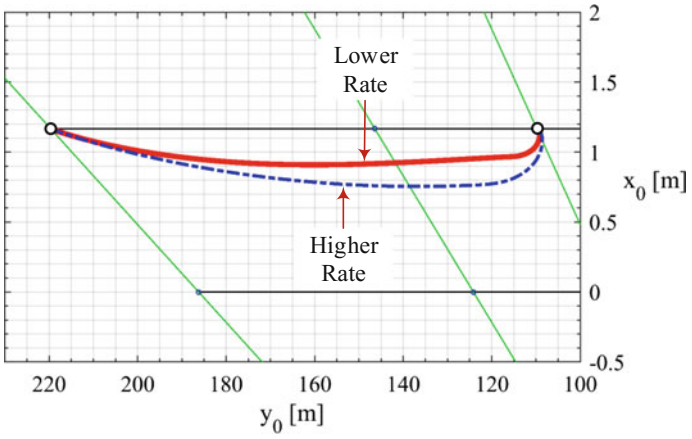

Fig. 1.22 Variation of ICR in body coordinate: effect of $\Delta\delta/\Delta t$ rate at constant v_x

1.3.3 Reference Road Profile

In Sect. 1.3.1, the time response of variables was shown to act very close to their steady-state solutions at each time sample. This step proves that the primary responses act lazily. Such a conclusion allowed us to continue a step further and see how the geometry of turning is affected by examining the location of ICR in Sect. 1.3.2. The transient location of ICR in body frame was shown to follow the ICR map with high level of similarity when the steer angle δ is kept constant while the vehicle accelerates. On the other hand, for variation of δ at constant forward velocity, the deviation between transient location and the ICR map is not that small. Although the scale of x in the ICR map plot is much larger than the scale of y, this deviation needs more investigation to be accepted as reasonably small. For this reason, in order to come up with a stronger conclusion about similarity of turning behavior between transient and QSS cases, we may continue one step further and examine the final path traveled by the vehicle to make a better judgment about the vehicle's behavior in turning maneuvers. As the path is, in fact, the coordinates of the vehicle's center of gravity in global frame, investigation of the path can be viewed as an equivalent to analyzing the ICR location in global frame.

In the previous sections, there was a QSS response defined for each pair of inputs (δ, v_x). In case of path, the QSS response will define an expected path with the given inputs. So, it would be more realistic for applications to start from a given intended path (instead of an expected path) and derive the required inputs (δ, v_x) which are expected to result in the intended path called the *reference road profile*. In fact, it is also highly reasonable to assume v_x to be known from the separately analyzed road in terms of safety considerations. Such safety considerations may include calculation of suggested speed range as a function of road curvature at any point on the road.

For a vehicle to stay on a given road at any time, ICR of the vehicle in global frame must coincide with the center of curvature of the road at that specific time [8]. As observed in Sect. 1.2, the ICR, whether expressed in body or global coordinates, moves on a smooth curve as the inputs to the vehicle change. In other words, there is no jump in the ICR location if the inputs are continuous. As a result, one expects continuous variation of rotation center of the traveled path as well. This implies that a feasible road profile must have continuous loci of center of rotation in global frame. Such a road profile might be feasible to be followed by a vehicle if the velocity and curvature conditions fit in the achievable limit. Such a feasibility limit may be translated to the following statement: "If the location of curvature center fits in the boundaries of Fig. 1.17 at every time, there will be a reasonably accurate solution for inputs (δ, v_x) to make the vehicle stay on the intended road."

A road with non-continuous loci of curvature center is theoretically impossible to be followed continuously. Although there will be approximate input solutions to keep the vehicle in an acceptable error boundary, but since there is discontinuity in the mathematical solution, the accuracy of path following will drop and sudden changes of inputs δ and/or v_x will also be necessary as an undesirable condition. Although the overall geometry of roads with continuous curvature do not visibly vary much from the ones with non-continuous curvature, but the consequences in vehicle control during maneuvering are critical. Note that different sections of the road might be tangent to each other, but have discontinuous curvature.

In the remaining sections we first design a proper sample road, and then use it as a reference road profile for the vehicle to follow.

Clothoid

For design of a road with continuous curvature, we need a mathematical function that acts as a transition curve between two steady-state curves (two circles or a circle and a line). Let us assume that the first section of the road is a circular curve with curvature $\kappa_1 = 1/R_1$ and the second section is another circle with curvature $\kappa_2 = 1/R_2$. Any of κ_1 or κ_2 may be zero in case of straight road.

A preferable transition between the two circular sections is the one with a constant increasing rate for κ with respect to the arc length. Such a transition also requires that beginning and end points coincide with the circular sections and the slope of the transition curve and departure and destination curves match each other. The solution to the constant rate of increase in curvature is the *Euler spiral* which is also called a *clothoid*. The parametric equation for a clothoid is given as [9]:

$$X(t) = a \int_0^t \cos\left(\frac{\pi}{2}u^2\right) du \tag{1.80}$$

$$Y(t) = a \int_0^t \sin\left(\frac{\pi}{2}u^2\right) du \tag{1.81}$$

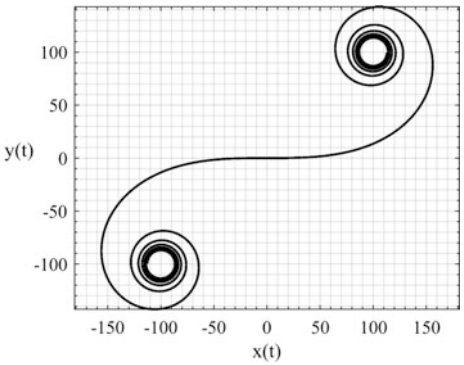

Fig. 1.23 Example of the Euler spiral

where the parameter a which defines the expansion of the curve, if we take t analogous to time, can be viewed as the speed of the pen that slides on the paper to draw the clothoid. One may convert the independent variable from t to arc length s by the following relationship:

$$s = at \tag{1.82}$$

The curvature and the slope of the clothoid along its length are also given as [9]:

$$\kappa = \frac{1}{R} = \frac{\pi t}{a} = \frac{\pi s}{a^2} \tag{1.83}$$

$$\theta = \frac{\pi}{2} t^2 = \frac{\pi s^2}{2a^2} \tag{1.84}$$

An example of a clothoid with $a = 200$ is plotted for $-5 < t < 5$ in Fig. 1.23 which is a representation of the Euler spiral.

Integrals of (1.80), (1.81) are known as Fresnel cosine and Fresnel sine integrals.

Sample Road 1

The first road profile is a road with a circular beginning with radius $R_1 = 160\,\text{m}$ and a second circular section with radius $R_2 = 80\,\text{m}$ at the end. These radii are calculated to approximately match the first scenario in Fig. 1.21. We start by calculating the transition clothoid and then match the circular paths with it, for simplicity. Assuming a constant value for $a = 200$ and using (1.83), (1.84), the clothoid expressions may be found by the following procedures to match the calculated curvatures in the beginning and at the end of the transition:

$$t_1 = \frac{\kappa_1 a}{\pi} = \frac{a}{\pi R_1} = 0.398, \qquad t_2 = \frac{\kappa_2 a}{\pi} = \frac{a}{\pi R_2} = 0.796 \tag{1.85}$$

$$\theta_1 = \frac{\pi}{2} t_1^2 = 0.249\,\text{rad}, \qquad \theta_2 = \frac{\pi}{2} t_2^2 = 0.995\,\text{rad} \tag{1.86}$$

$$X(t) = 200 \int_0^t \cos\left(\frac{\pi}{2} u^2\right) du \qquad (0.398 \leq t \leq 0.796) \tag{1.87}$$

$$Y(t) = 200 \int_0^t \sin\left(\frac{\pi}{2} u^2\right) du \qquad (0.398 \leq t \leq 0.796) \tag{1.88}$$

The centers of the curvatures at the beginning and at the end of the clothoid are located at:

$$X_{O1} = X(t_1) - R_1 \sin\theta_1 = 39.71\,\text{m} \quad Y_{O1} = Y(t_1) + R_1 \cos\theta_1 = 161.65\,\text{m} \tag{1.89}$$

$$X_{O2} = X(t_2) - R_2 \sin\theta_2 = 77.02\,\text{m} \quad Y_{O2} = Y(t_2) + R_2 \cos\theta_2 = 92.74\,\text{m} \tag{1.90}$$

Assuming the same t and a for the circular sections, the parametric equations of the circular sections are given as:

$$X(t) = X_{O1} + R_1 \cos\left(\frac{at}{R_1} + \alpha_0\right) \qquad (t_0 < t < 0.398) \tag{1.91}$$

$$Y(t) = Y_{O1} + R_1 \sin\left(\frac{at}{R_1} + \alpha_0\right) \qquad (t_0 < t < 0.398) \tag{1.92}$$

$$X(t) = X_{O2} + R_2 \cos\left(\frac{at}{R_2} + \beta_0\right) \qquad (0.796 < t < t_3) \tag{1.93}$$

$$Y(t) = Y_{O2} + R_2 \sin\left(\frac{at}{R_2} + \beta_0\right) \qquad (0.796 < t < t_3) \tag{1.94}$$

Intersecting the curves described in (1.87), (1.88) and (1.91), (1.92) at $t = t_1$ and doing the same for curves (1.87), (1.88) and (1.93), (1.94) at $t = t_2$ provides us with the values of α_0, β_0. We may then manually define the beginning point at $t_0 = -1$ and the end point at $t_3 = 3$ of the total road. Note that the independent variable t in the road design is different from the time it takes for the vehicle to travel the path and it is only used to create the reference path; thus, t might even take negative values as in here.

$$\alpha_0 = -1.82\,\text{rad} \tag{1.95}$$

$$\beta_0 = -2.57\,\text{rad} \tag{1.96}$$

$$t_0 = -1 \tag{1.97}$$

$$t_3 = 3 \tag{1.98}$$

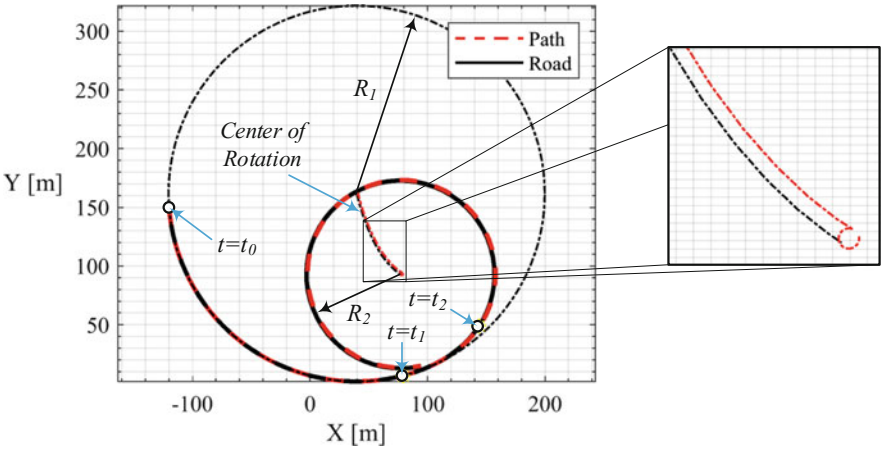

Fig. 1.24 Actual path of motion versus the reference road profile for road 1

Finally, the set of curves described in (1.87), (1.88) and (1.91)–(1.94) are used to draw the reference road profile *sample road 1* as shown in Fig. 1.24. Center of curvature in global frame at any point is also found and plotted from:

$$X_O(t) = X(t) - R(t)\sin\theta(t), \qquad Y_O(t) = Y(t) + R(t)\cos\theta(t) \tag{1.99}$$

where $\theta(t)$ and $R(t)$ are the slope and the radius of the curve at each point which depend on type of the curve at each section.

Sample Road 2

To further evaluate the idea, we introduce another road profile which generates a more complicated maneuver. Assume a straight road which eventually starts to bend in until it merges with a circular path. The road continues to almost complete a circle and then starts to decrease its curvature until it reaches back to its straight position so that it continues the same straight line in the beginning as shown in Fig. 1.25. Such a road is a good example for evaluating laziness of vehicles in maneuvering; if the calculated inputs to the vehicle cause considerable error, the vehicle will not get back to its initial orientation at the end of the road and we will observe an angle made between the initial and the final directions of motion.

The derivation of the road profile is similar to section "Sample Road 1". The second half of the profile may be calculated using a symmetry about the middle axis passing through the center of the circle. To be concise, the derivations are not described here and only the final equations of the curves are given:

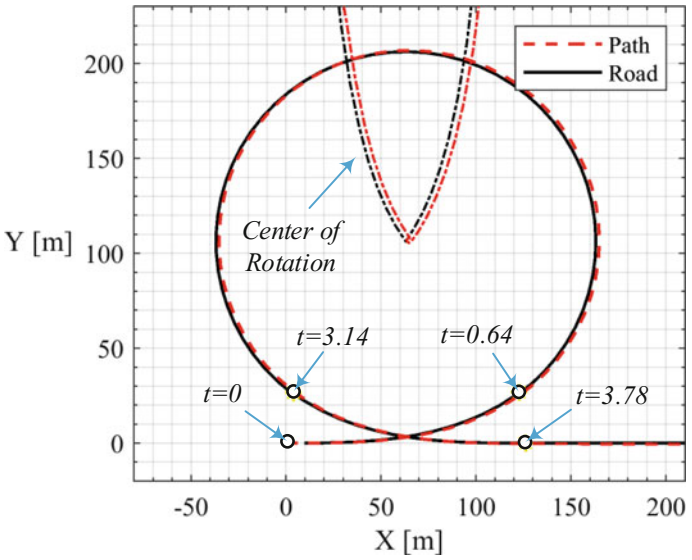

Fig. 1.25 Actual path of motion versus the reference road profile for road 2

$$X(t) = 200 \int_0^t \cos\left(\frac{\pi}{2}u^2\right) du \qquad (0 \le t \le 0.64) \qquad (1.100)$$

$$Y(t) = 200 \int_0^t \sin\left(\frac{\pi}{2}u^2\right) du \qquad (0 \le t \le 0.64) \qquad (1.101)$$

$$X(t) = 63.13 + 100 \cos\left(\frac{200t}{100} - 0.93\right) \qquad (0.64 < t < 3.14) \qquad (1.102)$$

$$Y(t) = 106.23 + 100 \sin\left(\frac{200t}{100} - 0.93\right) \qquad (0.64 < t < 3.14) \qquad (1.103)$$

$$X(t) = 126.25 - 200 \int_0^{3.78-t} \cos\left(\frac{\pi}{2}u^2\right) du \qquad (3.14 \le t \le 3.78) \qquad (1.104)$$

$$Y(t) = 200 \int_0^{3.78-t} \sin\left(\frac{\pi}{2}u^2\right) du \qquad (3.14 \le t \le 3.78) \qquad (1.105)$$

$$X(t) = 200t + 126.25 \qquad (t > 3.78) \qquad (1.106)$$

$$Y(t) = 0 \qquad (t > 3.78) \qquad (1.107)$$

1.3.4 Actual Path

The first step in determining the vehicle's path is to calculate the radius of curvature of the road at each point. Radius of curvature is calculated from (1.83) for clothoid sections and is a constant value for circular sections. The intended center of curvature at every point of the road may be translated into a desired ICR in body frame as in the ICR map in Fig. 1.17, if an allowable range of side-slip angle β is known as shown in Sect. 1.2.2, which can be used to solve for a non-unique pair of inputs (δ, v_x). In another approach, a constant velocity v_x may be assumed throughout the road by making sure that the centripetal acceleration required $a_c \approx v_x^2/R$ does not exceed the feasible limit of the vehicle. Then, the only unknown to be calculated is the steer angle δ and the problem is solved by obtaining a vector of δ associated with the vector of time t or distance traveled s. This may be done geometrically using Fig. 1.17 or using the curvature response S_κ from (1.40).

In this section, for road 1, we use the same constant velocity of $v_x = 20\,\mathrm{m/s}$ used in maneuver 1 of section "Manuver 1: Increasing Velocity". For road 2, we select the constant forward velocity of $v_x = 22\,\mathrm{m/s}$ considering the fact that the maximum centripetal acceleration required during the circular motion would be $a_c \approx v_x^2/R = 4.84\,\mathrm{m/s^2}$ which is below the limit of $4.91\,\mathrm{m/s^2}$.

Figure 1.24 and 1.25 show the actual path of the vehicle on road 1 and road 2 by inputting the steer angle calculated from the steady-state response. The location of ICR in global frame is also plotted with is calculated from (1.48), (1.49). It can be seen that the path of motion is very close to the reference road in both cases. These results show that there is a great agreement between path of motion of transient and QSS responses. It also shows that steady-state responses are well-suited for control of the vehicle and keep it on the road on properly designed roads, proving laziness of vehicles in turning maneuvers.

The maximum perpendicular distance (error) between the path and the road for road 1 is around 1 m and for road 2 is around 1.5 m which are negligible compared to the radii of roads. It also shows that the vehicle will almost stay inside the intended lane, which is typically around 3 m wide.

It is important to note that there is a visible difference between the center of curvature of the road and global ICR location which is almost eliminated in the path of motion. Such a deviation in rotation centers is due to the fact that the heading direction of the vehicle is not necessarily tangent to the road. In other words, there is a nonzero side-slip angle β present, as expected from Fig. 1.10, that causes ICR to rotate on a circle instead of staying at a fixed point, at steady-state. The value of the side-slip angle is dictated by the imposed forward velocity v_x as discussed in Sect. 1.3.2; however, radius of rotation of the vehicle and the path are equal at steady-state. Figure 1.26 shows this in more detail in an exaggerated manner.

To see the effect of reference velocity v_x on the imposed side-slip angle β and ICR deviation from road center of curvature, we may conduct the same simulation on road 1 with different forward velocities and plot them together as shown in Fig. 1.27.

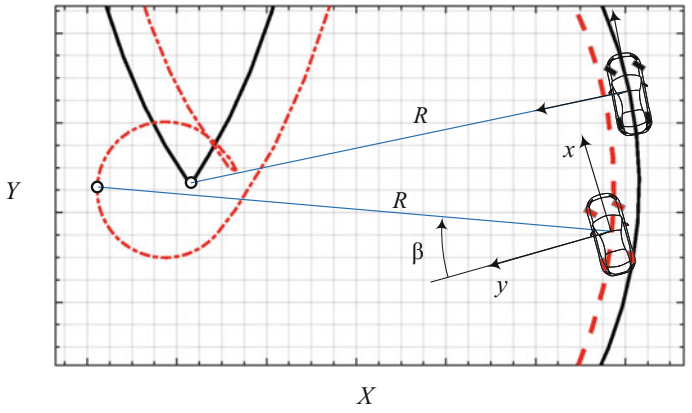

Fig. 1.26 Detailed view of the side-slip angle while maneuvering on the road

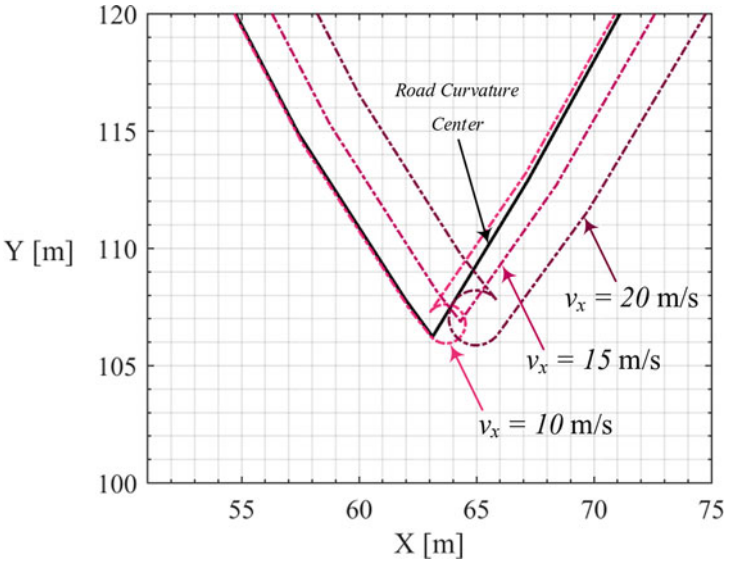

Fig. 1.27 Effect of v_x on side-slip angle β and ICR deviation

It can be seen in Fig. 1.27 as the velocity gets closer to the zero side-slip velocity explained in Sect. 1.3.2, the deviation of ICR from road center of curvature is decreased, implying that the vehicle is moving with more similar heading direction to the road. The side-slip angle is positive for $v_x = 10$ m/s, zero for $v_x = 15$ m/s, and negative for $v_x = 20$ m/s.

1.4 Summary and Conclusions

The objective of this chapter was to show how close vehicles act to their steady-state when undergoing a transient maneuver in normal driving conditions. The well-known bicycle model was chosen to simulate vehicle behavior as it has proven to be a reasonable approximate modeling for normal driving conditions with relatively low accelerations and slip angles. Detailed equations of motion of the bicycle model were given in Sect. 1.1 and steady-state solutions were extracted and summarized in Eqs. (1.21)–(1.24) and (1.40). Calculations of curvature, turning radius, the location of instantaneous center of rotation, and the calculation of path of motion were explained in Sect. 1.2.

In Sect. 1.3.1, transient and quasi-steady-state solutions were compared in time domain for two main transient maneuvers which reveal the overall behavior of the vehicle variables in time domain and also in inputs' domain using surface maps. The similarity between the transient and quasi-steady-state responses were promising, except v_y response when δ was increasing, and we concluded that overall vehicle behavior is lazy in turning maneuvers between two steady-states, as the major activity in normal driving.

Investigation on the laziness of vehicles needed more evaluation on the next level of vehicle response, namely the location of instantaneous center of rotation. This investigation was performed in Sect. 1.2 by calculating body and global expressions of the point. A useful chart was presented in Sect. 1.3.2 as the "ICR map" of a vehicle. The concept of tangent point was explained in detail, clarifying the quality of turning maneuver with geometrical expressions. Examples of basic transient maneuvers were also investigated on the "ICR map" and it was found that the vehicles also act lazy in that regard, specially when forward velocity changes at constant steer input.

For better understanding the vehicle's behavior when the steer angle changes, road profile and its creation as an expected path of motion were discussed in Sect. 1.3.3 and two sample roads were designed. Such road profiles enabled us to apply an open loop steering control algorithm based on steady-state responses and the results were satisfying, justifying that vehicles are lazy during turning maneuvers in normal driving conditions. It was also found that although the instantaneous center of rotation of the vehicle and the curvature center of the road may not exactly coincide because of the velocity and side-slip relation, the path-following error is kept minimum. It is important to note that such a conclusion does not imply that vehicle path following can be simply achieved by an open-loop control strategy, as vehicles may be driven at more severe circumstances at specific moments. Also, the availability of road and vehicle data, vehicle variable measurements, etc. with high-certainty is not guaranteed, the vehicle model might include unmodeled dynamics, and roads might be imperfectly designed.

As a result, it is concluded that steady-state responses, including the maps presented in this document, may be used as a feed-forward strategy to strongly enhance control quality with high accuracy; second usage of steady-state responses is to get

insight about vehicle's maneuvering behavior and possible operating ranges; another important usage is to design roads based on steady-state characteristic of vehicles. In parallel to steady-state feed-forward control, a feedback control is always needed to compensate for errors caused by different sources including uncertainties and unmodeled dynamics. Such a feedback control in a path-following strategy might be tuned to keep the vehicle in a boundary around the road profile at each time instant, such as a lane width.

List of Symbols

α_i	Tire side-slip angle for tire number i
β_i	Body side-slip angle at the center of wheel number i
v_x	Longitudinal velocity of center of gravity in body frame
v_y	Lateral velocity of center of gravity in body frame
v_{yi}	Lateral velocity of wheel center i in body frame
v	Total velocity of center of gravity
δ	Steer angle
$C_{\alpha i}$	Cornering stiffness of tire number i
m	Vehicle's mass
a_1	Distance from center of gravity to front axle
a_2	Distance from center of gravity to rear axle
l	Wheelbase
I_z	Yaw moment of inertia
F_{yi}	Lateral force of tire number i
F_y	Total lateral force at center of gravity
M_z	Total yaw moment at center of gravity
S_y	Lateral velocity response
S_r	Yaw velocity response
S_β	Side-slip response
S_a	Lateral acceleration response
S_κ	Curvature response
a_x	Forward acceleration in body frame
a_y	Lateral acceleration in body frame
a_c	Centripetal acceleration
K	Stability factor
R	Radius of curvature
κ	Curvature
${}^G R_B$	Rotation matrix from body to global frame
x_0, y_0	Coordinates of instantaneous center of rotation in body frame
X_0, Y_0	Coordinates of instantaneous center of rotation in global frame
X_C, Y_C	Coordinates of center of gravity global frame
X, Y	Road profile coordinates in global frame
X_O, Y_O	Coordinates of road center of curvature in global frame

References

1. Ellis, J. (1969). *Vehicle dynamics*. Business Books.
2. Milliken, W. F., & Milliken, D. L. (1995). *Race car vehicle dynamics*. Warrendale, PA: Society of Automotive Engineers.
3. Jazar, R. N. (2017). *Vehicle dynamics: Theory and application*. Berlin: Springer.
4. Van Zanten, A. T. (2000). *Bosch esp systems: 5 years of experience*. SAE Technical Paper.
5. Rajamani, R. (2011). *Vehicle dynamics and control*. Berlin: Springer.
6. Marzbani, H., Vo, D. Q., Khazaei, A., Fard, M., & Jazar, R. N. (2017). Transient and steady-state rotation centre of vehicle dynamics. *International Journal of Nonlinear Dynamics and Control, 1*(1), 97–113.
7. Jazar, R. N. (2011). *Advanced dynamics: Rigid body, multibody, and aerospace applications*. London: Wiley.
8. Jazar, R. N. (2010). Mathematical theory of autodriver for autonomous vehicles. *Journal of Vibration and Control, 16*(2), 253–279.
9. Marzbani, H., Jazar, R. N., & Fard, M. (2015). Better road design using clothoids. In: *Sustainable automotive technologies 2014* (pp. 25–40). Berlin: Springer.